Clim Dyn (2011) 37:325–341
DOI 10.1007/s00382-010-0923-y

Sensitivity of the tropical Pacific seasonal cycle and ENSO to changes in mean state induced by a surface heat flux adjustment in CCSM3

Xiaohua Pan · Bohua Huang · Jagadish Shukla

Received: 11 December 2009 / Accepted: 27 September 2010 / Published online: 28 October 2010

Abstract The influence of mean climate on the seasonal cycle and the El Niño-Southern Oscillation (ENSO) in the tropical Pacific climate is investigated using the Climate Community System Model Version 3 (CCSM3). An empirical time-independent surface heat flux adjustment over the tropical ocean is applied to the oceanic component of CCSM3. In comparison with the control run, the heat flux-adjusted run simulates a more realistic mean climate not only for the sea surface temperature (SST) but also for wind stress and precipitation. Even though the heat flux adjustment is time-independent, the seasonal cycles of SST, wind stress and precipitation over the equatorial eastern Pacific are more realistic in the flux-adjusted simulation. Improvements in the representation of the ENSO variability in the heat flux-adjusted simulation include that the Nino3.4 SST index is less regular than a strong biennial oscillation in the control run. But some deficiencies also arise. For example, the amplitude of the ENSO variability is reduced in the flux-adjusted run. The impact of the mean climate on ENSO prediction is further examined by performing a series of monthly hindcasts from 1982 to 1998 using CCSM3 with and without the heat flux adjustment. The flux-adjusted hindcasts show slightly higher predictive skill than the unadjusted hindcasts with January initial conditions at lead times of 7–9 months and July initial conditions at lead times of 9–11 months. However, their differences during these months are not statistically significant.

Keywords Mean climate · Seasonal cycle · ENSO · CCSM3 · Heat flux adjustment · Pacific Ocean

X. Pan · B. Huang · J. Shukla
Center for Ocean–Land–Atmosphere Studies, Institute of Global Environment and Society, Calverton, MD, USA

X. Pan · B. Huang · J. Shukla
Department of Atmospheric, Oceanic and Earth Sciences, George Mason University, Fairfax, VA, USA

Present Address:
X. Pan
Goddard Earth Science Technology Center, University of Maryland at Baltimore County, Baltimore, MD, USA

X. Pan (✉)
NASA GSFC Code 613.3, 20771 Greenbelt, MD, USA
e-mail: xiaohua.pan@nasa.gov

1 Introduction

ENSO is generally understood as a low-frequency fluctuation superimposed on a mean climate over the tropical Pacific (Bjerknes 1969) where the mean climate is defined as the long-term average of the system. Figure 1a shows the observed mean climate of sea surface temperature (SST) for the period of 1900–1999 and surface wind stress for the period of 1948–2003 in the tropical Pacific (data source is listed in Sect. 2.2). The mean SST features a well-known east–west asymmetry near the equator, with a cold tongue in the eastern Pacific and a warm pool in the western Pacific accompanied by easterly trade winds. A north–south asymmetry is present in the eastern Pacific where warm water is located in the north of the equator and the cold tongue is present on the equator and along the coast of Peru, with the cross-equatorial southerly trade winds straddling in between.

The asymmetric structures in mean climate are substantially weakened in current coupled ocean–atmosphere general circulation models (CGCMs) (e.g., Davey et al. 2002). The north–south asymmetry in the eastern equatorial

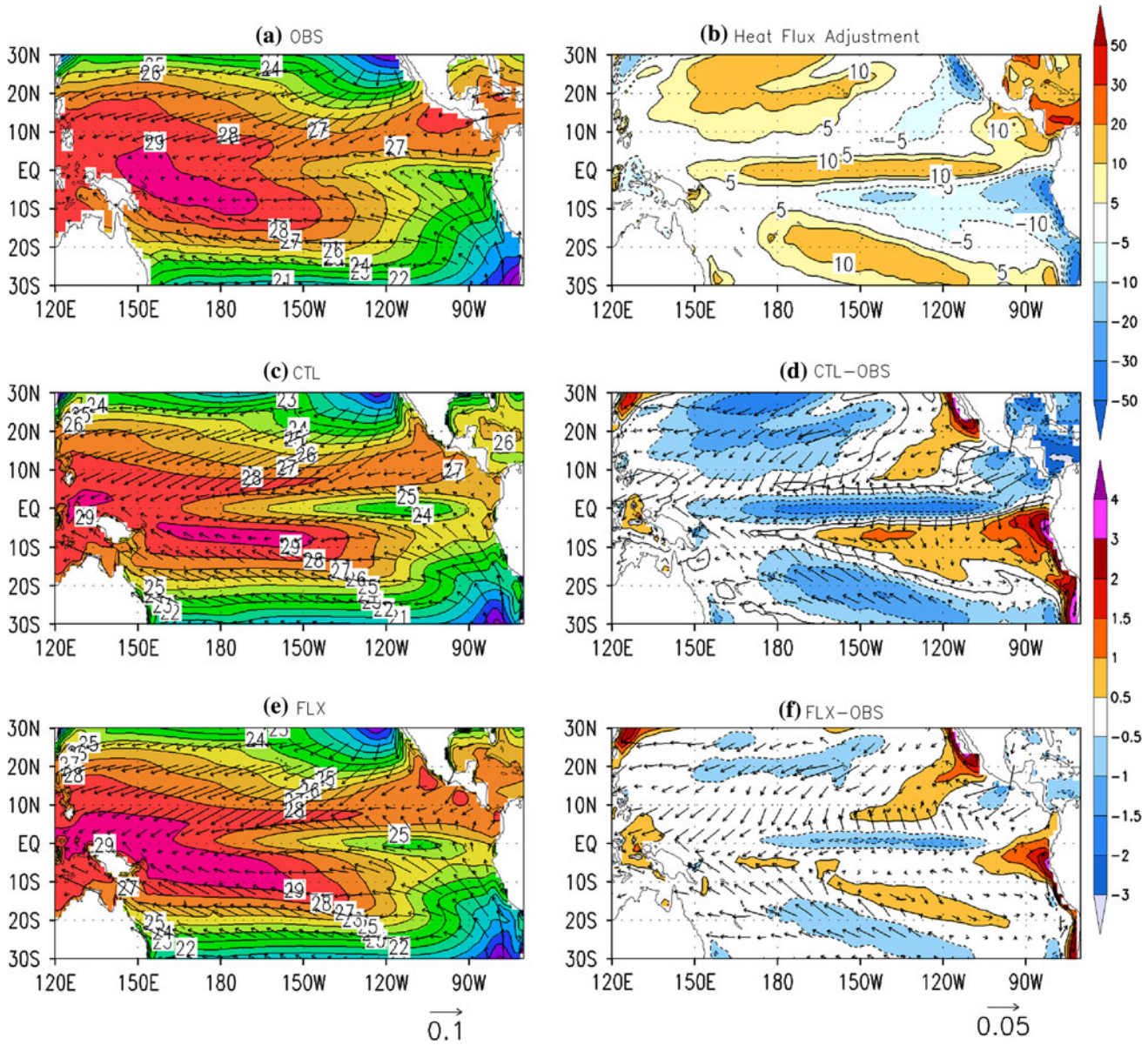

Fig. 1 Spatial distributions of mean climate SST (°C) and wind stress vector (N m^{-2}) over the tropical Pacific for **a** OBS, **c** CTL, **d** bias of CTL, **e** FLX and **f** bias of FLX. The *shadings* represent SSTs and *vectors* represent wind stress with the magnitude of 0.1 N/m^2 in the *left panels* and 0.05 N/m^2 in the *right panels*. **b** Spatial distribution of the heat flux adjustment term with the conversion coefficient $R = 10$ over the tropical Pacific. Unit is W m^{-2}. Positive values mean adding heat flux to ocean. The observed SST is from Hadley1.1 SST analysis for the period of 1900–1999. The observed surface wind stress is from NCEP–NCAR Atmospheric Reanalysis 1 for the period of 1948–2003. CTL is for period of 1900–1999. FLX is for the period of 1945–1994

Pacific is weakened due to the warm bias near the coast of Peru. As a result, the model mean SST field becomes more suitable for the existence of a robust double inter-tropical convergence zone (ITCZ) (e.g., Lin 2007) since the moist convection parameterizations in the current models produce convection over unrealistically warm water to the south of the equator. The east–west asymmetry is also substantially weakened due to the cold SST bias in the central equatorial Pacific and the warm bias near the coast of Peru in many CGCMs.

Besides the mean state biases, current CGCMs also show major errors in tropical variability from seasonal to interannual time scales. It is quite common that the seasonal cycles in the eastern equatorial Pacific in these CGCMs are either underestimated or dominated by a semiannual cycle (Mechoso et al. 1995; Latif et al. 2001). Two kinds of problems seem to stand out in ENSO simulations by current coupled systems, especially in CCSM3 (e.g., Latif et al. 2001; AchutaRao and Sperber 2002; Davey et al. 2002; Joseph and Nigam 2006; Annamalai et al.

2007; Leloup et al. 2008). Temporally, the simulated ENSO cycle is more regular than the observed one and ENSO events tend to occur too frequently in the models. Spatially, the SST anomalies in the tropical Pacific extend too far westward and are too narrowly confined to the equatorial zone.

Therefore, it is natural to ask whether the deficiency in the simulation of seasonal cycle and ENSO is associated with the deficiency in mean climate, in particular the warm biases near the coast of Peru, cold biases in the central equatorial Pacific and the double ITCZ. The influence of mean climate on the ENSO characteristics in a model simulation has been studied previously. Theoretical work done by Zebiak and Cane (1987) showed that the structure of mean climate has an impact on the ENSO amplitude and period in their model. In order to investigate the influence of mean climate on the ENSO variability in CGCMs, Li and Hogan (1999); Spencer et al. (2007), and Manganello and Huang (2009) applied an annual-mean heat flux or wind stress adjustments in certain coupled CGCMs to reduce the mean climate biases. Although the mean climates were significantly improved in all three studies, their influences on the ENSO simulation turned out to be diverse. Spencer et al. (2007) found that ENSO variability was suppressed when a heat flux adjustment was applied in the tropics wide while enhanced when applied only within 10° of the equator. Neither these heat flux adjustments nor a wind stress adjustment alone improved the ENSO variability in their CGCM. In contrast, the other two studies found that the representation of ENSO was improved by heat flux adjustments in their models. Li and Hogan (1999) found that interannual variability was more realistic after the mean climate was improved by implementing an annual mean adjustment either for SST alone or both for SST and wind stress. With an annual mean heat flux adjustment, Manganello and Huang (2009) also found the phase relationship between ENSO and the seasonal cycle in their CGCM was improved. Therefore, it is necessary to examine a wider range of the coupled systems to get further insight into this question and to understand the sources of the model diversity. This study is an attempt in this direction.

In this study, our hypothesis is as follows: if the mean climate in a coupled model is improved significantly, it will have positive impacts on the seasonal cycle, ENSO simulation and predictability of the model. In order to test this hypothesis, a time-independent (i.e. annual-mean) surface heat flux adjustment scheme is implemented to reduce the mean climate SST biases in a coupled model. This method is similar to the above studies. Complementary to the previous studies discussed above, we used the Climate Community System Model version3 (CCSM3) in this study. This coupled model is developed at the National Center for Atmospheric Research (NCAR). Compared with the coupled models used in previous studies, CCSM3 is more state-of-the-art, with a higher resolution for both the atmospheric and oceanic components, and more recent sub-scale physical parameterizations. Using this model, we investigate the influence of mean climate not only on the seasonal cycle and ENSO simulation but also on ENSO prediction. To this end, a set of hindcasts is performed with both January and July initial conditions for a period of 17 years, so that the seasonal dependence of prediction skill can be evaluated. This set of hindcasts includes more cases than those considered by Manganello and Huang (2009).

The paper is organized as follows. Section 2 describes CCSM3 component models and the observational data used to assess the model results. Section 3 describes the design of the sensitivity experiments to examine the impact of mean climate on ENSO simulation and prediction. The modified mean climate and its influence on the seasonal cycle are discussed in Sect. 4. The influences of the flux-adjusted mean climate on ENSO simulation and prediction are discussed in Sects. 5 and 6, respectively. The summary, conclusion and discussion are presented in Sect. 7.

2 Model and observational data

2.1 Model

CCSM3 is an earth system model comprised of four components, each for the atmosphere, ocean, land and sea ice. These components interact with each other through a flux coupler. The atmospheric model is the Community Atmosphere Model Version 3 (CAM3), and the land surface model is the Community Land Surface Model Version 3.0 (CLM3). The sea ice model is the Community Sea Ice Version 5.0 (CSIM5) and the ocean model is the Parallel Ocean Program version 1.4.3 (POP). The major features of each of these components have been described in detail by Collins et al. (2006). Here, we discuss only a few aspects of particular relevance to our study.

In this study, CAM3 and CLM3 have a horizontal resolution of T85, corresponding to a spatial resolution of 1.4°. CAM3 has 26 vertical levels. The spacing of POP and CSIM5 grids is 1.125° in the zonal direction and roughly 0.5° in the meridional direction with higher resolution near the equator. The vertical dimension is treated using a depth (z) coordinate with 40 levels extending to 5.37 km. POP employs an isopycnal sub-scale tracer transport parameterization, anisotropic horizontal viscosity, the non-local K-profile parameterization (KPP) vertical mixing, and an idealized diurnal cycle of solar forcing. Air–sea coupling is accomplished by passing the latent, sensible, and radiative heat flux, fresh water and momentum flux between the

ocean and atmosphere components periodically and conservatively. The standard CCSM3 uses a 1-day coupling interval for the ocean model, and a 1-h coupling for the other components of the coupled system. At the end of each ocean coupling interval, the oceanic component sends its time averaged, upper level (10 m) temperature and velocity to the flux coupler, which takes these to be the SST and the surface current. After every 1-h radiation calculation, the atmospheric component sends the coupler the fluxes of net surface solar and long-wave radiation along with the averaged wind speed, potential temperature, humidity, density, precipitation and geopotential height at its lowest model level to the coupler. Using these inputs from the oceanic and atmospheric components, the coupler generates the turbulent momentum, heat and fresh water fluxes on hourly basis and then averages these fluxes to daily means before passing these quantities on to force the oceanic component once every 24 h.

2.2 Observational datasets

In order to validate the results from the model, several observation-based monthly analyses (denoted by OBS) are used to calculate the mean climate, seasonal cycle and ENSO variability. We use global Hadley1.1 SST analysis (1900–1999) produced by the Hadley Centre (Rayner et al. 2003). The fields of surface wind stress and sea level pressure (1948–2003) are from the National Centers for Environmental Predictions–National Center for Atmospheric Research (NCEP–NCAR) Atmospheric Reanalysis 1 (Kalnay et al. 1996). The precipitation (1979–2005) is from the Climate Prediction Center (CPC) Merged Analysis of Precipitation (CMAP) (Xie and Arkin 1997), based on blended satellite and in situ measurements. The oceanic heat content is defined as the ocean temperature averaged over the top 300 m. This is also used as a proxy for the thermocline depth. To initialize and evaluate the ENSO hindcasts, we use the three-dimensional fields of oceanic temperature, salinity, and current (1980–1998) produced by the ocean data assimilation (ODA) from Geophysical Fluid Dynamics Laboratory (Derber and Rosati 1989).

3 Experimental design

3.1 Heat flux-adjusted simulation

The thermodynamic equation governing the SST can be simplified as

$$\frac{\partial(\mathrm{SST})}{\partial t} \propto [Q_0 + Q_\mathrm{D}]. \tag{1}$$

The tendency of SST is mainly determined by two processes: the contribution from the net local air–sea heat exchange (Q_0) that includes the solar and longwave radiation, sensible and latent heat flux (a function of SST among other factors), and the contribution from the oceanic heat transports (Q_D) that include horizontal and vertical temperature advections, entrainment of cold water into the oceanic mixed layer, sub-scale temperature diffusion, and the penetrating solar radiation through the bottom of the mixed layer. In long-term mean, i.e., $\frac{\partial(\mathrm{SST})}{\partial t} \sim 0$, the balance among these processes determines the mean SST. A model SST bias arises from the systematic errors in Q_0 and Q_D. Due to the complicated feedback processes, the sources of the systematic errors are yet to be clearly identified. In this study, we hypothesize that a major part of the error is from the local heat flux into the ocean, such as the excessive shortwave radiative flux at the sea surface due to inadequate cloud absorption near the Peru coast. To reduce the effect of such error sources, a sensitivity run is performed in which a time independent surface heat flux adjustment term (ΔQ) is added to the right hand side of Eq. 1 to compensate for the systematic error. The new thermodynamic equation is given as

$$\frac{\partial(\mathrm{SST_{new}})}{\partial t} \propto [Q_0 + Q_\mathrm{D} + \Delta Q], \tag{2}$$

where ΔQ is defined empirically as

$$\Delta Q = -\Delta\mathrm{SST} \times R, \tag{3}$$

where ΔSST is the 100-year (1900–1999) mean climate SST bias of the control run in comparison with the observations (refer to Fig. 1d) and R is a conversion coefficient. Note that the surface heat flux adjustment term is constant in time in this study; in other words, the additional heat flux is only a function of space, so that it will not directly influence oscillatory variations, such as the seasonal cycle in the model. In this study, the surface heat flux adjustment is applied within 30° of the tropics in both hemispheres. Its value decreases to zero linearly from 30° to 40° in both hemispheres. This adjustment is used in both the simulation and hindcasts that are described later.

It should be noted that $\frac{\partial(\mathrm{SST})}{\partial t}$ is non-zero due to the climate change. Yet in designing the heat flux adjustment term, we assume that $\frac{\partial(\mathrm{SST})}{\partial t}$ is negligible in long-term mean. In the tropical region, e.g. the southeastern Pacific, the bias induced by systematic error is as much as 3°C and quickly overwhelms the change caused by the greenhouse gases. A very similar pattern of bias is also found in the preindustrial simulations (i.e. simulations without changing greenhouse gases). Therefore, we confine our flux adjustment to within the tropics region and assume that the change of SST induced by the greenhouse gases there is negligible.

The conversion coefficient (R) is adjustable and has a unit of Watts per meter square per Kelvin, i.e. W m^{-2} K^{-1}.

It is used to convert the unit of SST biases from temperature into the unit of energy. In order to test the sensitivity of the mean climate on the value of the conversion coefficient R, flux adjustment experiments with different values of R were examined. Since the heat flux changes approximately 15 W m^{-2} in a fully coupled model given an SST change of 1 K (Doney et al. 1998), we test R with values of 10 and 15 W m^2 K^{-1}. $R = 10$ gives a better mean SST and is chosen for the experiments. Figure 1b gives the spatial distribution of the heat flux adjustment term ΔQ in a unit of W m^{-2} with $R = 10$, calculated from the mean SST error of a 100-year CCSM3 simulation to be described in the next paragraph. Using this value for the conversion coefficient, heat with values more than 10 W m^{-2} is added into the equatorial Pacific to compensate for the cold SST bias there. Similarly, more than 30 W m^{-2} of heat is removed from the ocean along the coast of Peru to reduce the warm SST bias. In the open ocean of the subtropics, about 10 W m^{-2} of heat are added. Along the equatorial Pacific (averaged between 5°S–5°N), a heating effect of average 5–10 W m^{-2} is added to the ocean to the west of 110°W, while a cooling effect is applied to the ocean to the east of 110°W with its magnitude sharply increasing eastward from zero to 30 W m^{-2}.

The heat flux-adjusted simulation using the above heat flux adjustment scheme and the unadjusted simulation (i.e. the control simulation) are hereafter referred to as the FLX and CTL simulations, respectively. CTL, used for calculating ΔQ, is a 100-year simulation from the first run (run 1 out of 9) of the twentieth century experiments in the Intergovernmental Panel on Climate Change/phase 3 of the Coupled Model Intercomparison Project multi-model dataset (IPCC/CMIP3). Its output is taken from the multi-model datasets (see http://www-pcmdi.llnl.gov/ipcc/about_ipcc.php; Meehl et al. 2005) from January 1900 to December 1999. Note that the output of CTL corresponds to actual years of the twentieth century because it is forced by observed twentieth century greenhouse gases and volcanic forcing. FLX is a 55-year integration in which a heat flux adjustment term is applied as described above. This run is initialized from the instantaneous CTL atmospheric and oceanic state on January 1, 1940. To eliminate the transient response to the heat flux adjustment at the beginning of the run, the first 5 years of FLX are used to spin up the system and only the last 50 years are used to conduct the analyses. As seen later in this paper, after the first 5 years the model upper ocean reaches a quasi-equilibrium state, with steady ENSO variability superimposed upon it. Although the length of model integration for FLX is only half of that for CTL due to the limitation of computational resources, it seems adequate to study the interannual variability like ENSO. As CTL, FLX is also labeled as actual years for the same reason.

It is important to note that the global average of the heat flux adjustment term is about 1.74 W m^{-2}, i.e. non-zero, in our study. But this net heat input imposed by the heat flux adjustment does not cause a major climate shift or long-term drift. The heat flux adjustment, through initiating modest changes in SST and surface wind, generates an adjustment of the other surface heat flux components, i.e. the latent, sensible, and the long wave radiative heat fluxes. As a result, a new surface heat balance is quickly reached within a few years. In order to exclude the effect from the heat flux adjustment, we remove the first 5 years of the simulation from the analysis as mentioned earlier. Our analysis shows that the globally time averaged net heat flux is -1.78 W m^{-2} for the observations (should be zero, caused by systematic error in measurement), 0.51 W m^{-2} for CTL and -0.74 W m^{-2} for FLX. Hence the magnitudes of both the heat flux adjustment and the net heat flux from FLX are qualitatively similar to those from the observations and CTL within a range of a measurement uncertainty.

3.2 Heat flux-adjusted hindcasts

In order to assess the impact of the mean climate on ENSO prediction and predictability, a series of monthly hindcast experiments are performed using CCSM3 with and without the heat flux adjustment, denoted as the FLX and CTL hindcasts, respectively. Since the predictability of ENSO is seasonally dependent (Latif et al. 1994), two sets of hindcasts with initial conditions at different seasons are performed. One set is initialized on January 1 and the other on July 1 of each year from 1982 to 1998. Each hindcast is integrated for 12 months. Given that atmospheric initial conditions are not as important as the ocean initial conditions in the tropics for the purpose of seasonal forecasts (Shukla 1998), an ensemble of three hindcasts is generated by perturbing only the initial conditions of the atmosphere (land and sea ice as well) that are taken from the 50-year FLX simulation. The ocean initial condition for each ensemble member is identical. It is interpolated from the GFDL ocean assimilation data based on MOM3 using a variational optimal interpolation scheme. The detailed ocean initialization strategy has been described by Kirtman and Min (2009). It is important to note that initial conditions of the atmosphere, land, sea ice and ocean in FLX hincasts are identical to those in their CTL counterparts.

4 Mean climate and seasonal cycle

In this section we compare the results from the 50-year heat flux-adjusted run (i.e. FLX) with the 100-year control run (i.e. CTL) and the observations in terms of mean climate

and the seasonal cycle. The full lengths of the observed datasets (described in Sect. 2.2) are used for the comparison.

4.1 Mean climate

Figure 1c–f shows the annual mean SST and wind stress in the 100-year CTL and the 50-year FLX and their differences from the observations in the tropical Pacific. The simulated annual mean SST is significantly improved in FLX relative to CTL (Fig. 1d, f). For example, the equatorial cold bias is reduced by about 0.5°C, and extends less towards the western Pacific in FLX relative to CTL. The warm bias off the coast of South America is also less pronounced, and is about 0.5°C closer to the observations. Away from the equator, the cold bias is reduced by 0.5–1°C.

It should be noted that the simulated annual mean wind stress and precipitation are also improved in FLX relative to CTL without any adjustments to momentum and fresh water fluxes applied. These improvements are due to the model dynamical responses to the changes in SST. The cross-equatorial southerly wind near the coast of South America, which is crucial to form the cold tongue there (Fig. 1a), is largely underestimated in CTL (Fig. 1c) but comparable to the observations in FLX (Fig. 1e). Figure 2 shows the mean precipitation in tropical Pacific. Although both CTL and FLX have large systematic errors of double ITCZ due to the South Pacific convergence zone (SPCZ) extending too far eastward and northward with excessive precipitation, the double ITCZ is reduced in FLX (Fig. 2e, f) in comparison to CTL (Fig. 2c, d). This improvement corresponds to the reduced warm bias and more realistic southerly winds near South America in FLX (refer to Fig. 1e, f). It is also found that the entire equatorial, especially near Central America, is less dry in FLX than in CTL (Fig. 2b). This improvement corresponds to the reduced cold bias along the equatorial Pacific (Fig. 1d, f).

A possible explanation for the improvement in the southeastern Pacific (10°S–10°N, zonally averaged over 120°E–80°W) can be drawn from Fig. 3, which gives the comparison of CTL (in blue), FLX (in red) and OBS (in black) in terms of time-averaged SST, SLP and meridional wind stress in the southeastern Pacific. As shown in Fig. 1b, heat is taken away from the ocean in the Peru coastal region but put into the ocean over Central America at a fixed rate. This persistent heat flux adjustment tends to reduce warm biases in the south of the equator and cold biases in the north of the equator in FLX relative to CTL (Fig. 3a). Following the changed SSTs, air masses near the sea surface become colder and denser in the south but get warmer and lighter in the north, which in turn leads to higher SLP in the south but lower SLP in the north (Fig. 3b). The enhanced northward pressure gradient force across the equator is established. It then causes stronger cross-equatorial southerly winds, as the Coriolis force is

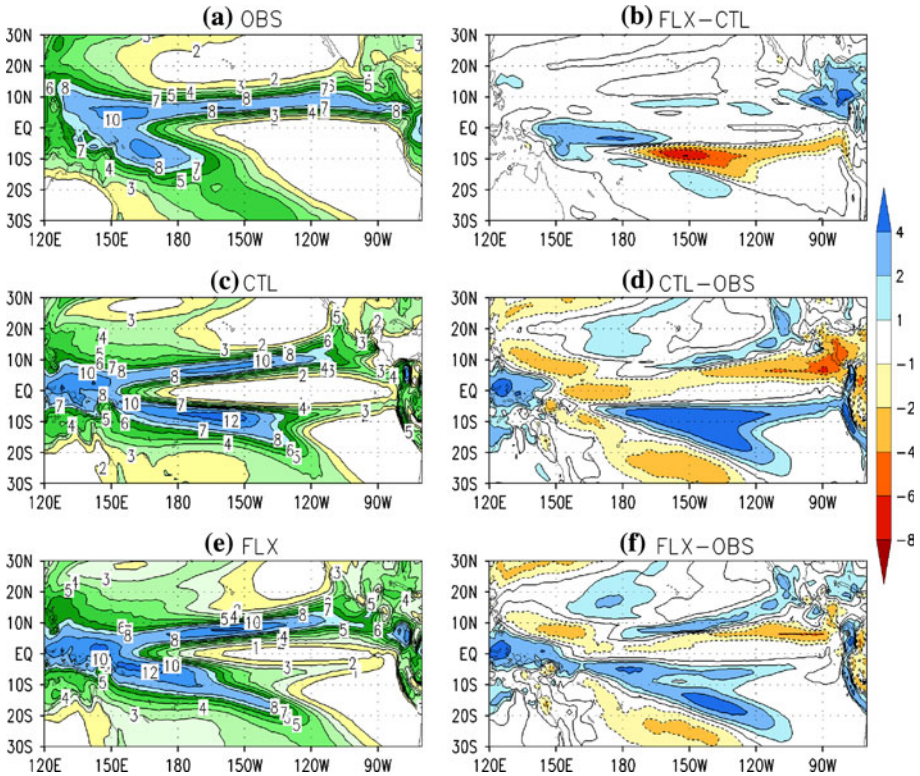

Fig. 2 Spatial distributions of mean climate precipitation (mm day^{-1}) over the tropical Pacific for **a** OBS, **b** FLX-CTL, **c** CTL, **d** bias of CTL, **e** FLX, **f** bias of FLX. The *color bar* is only for **b**, **d** and **f**. The observed precipitation is from CMAP for the period of 1979–2005. CTL is for period of 1900–1999. FLX is for the period of 1945–1994

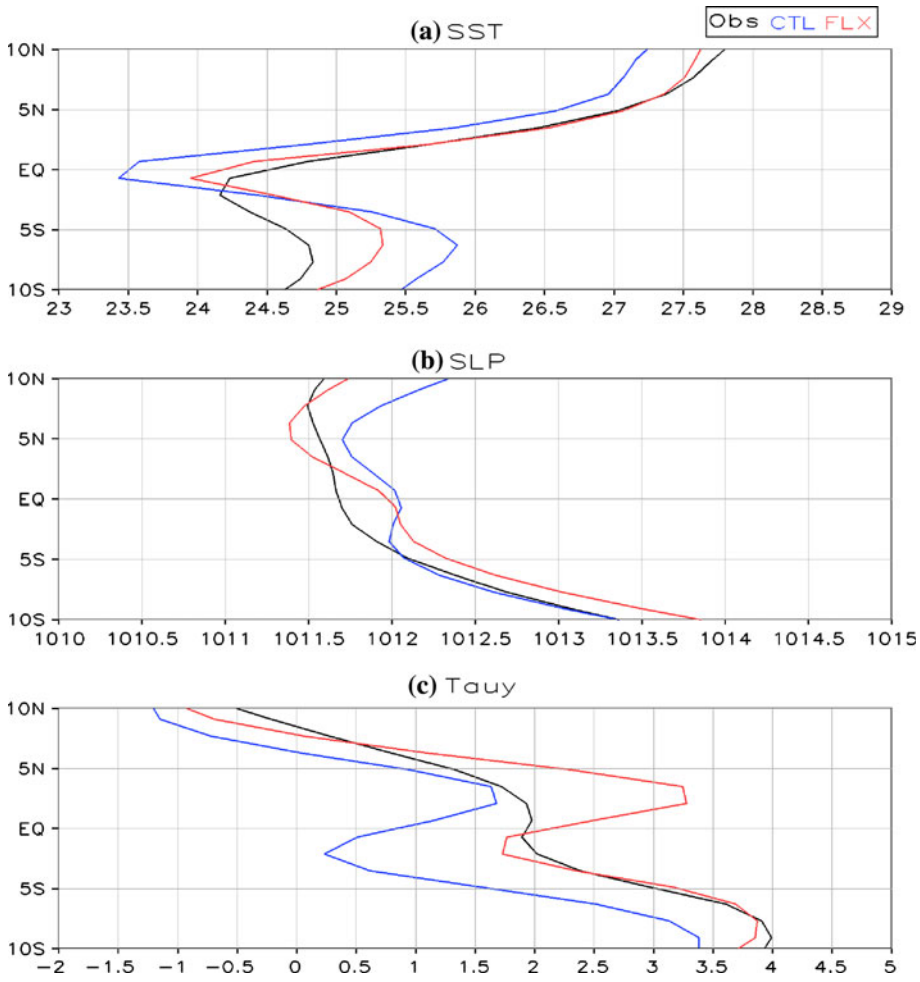

Fig. 3 Comparison of CTL (in *blue*), FLX (in *red*) and OBS (in *black*) in terms of mean climate **a** SST (°C), **b** SLP (mb) and **c** meridional wind stress (0.01 N m^{-2}) in the eastern Pacific (zonally averaged over 120°W–80°W)

very small in this area (Fig. 3c). Although this chain of reactions, as mentioned above, is initially triggered by the imposed heat flux adjustment, a positive feedback may follow suit because the corresponding change in the surface winds tends to reinforce the initial SST contrast by influencing both oceanic evaporation and mixing near the sea surface. Therefore, the positive wind-evaporation-sea surface temperature feedback, triggered by the heat flux adjustment, physically contributes to the achievement of a new equilibrium (or mean) state that has a more realistic north–south asymmetric structure in the eastern Pacific.

4.2 Seasonal cycle

The seasonal cycles of 100-year CTL, 50-year FLX and observations are calculated in the equatorial Pacific (120°E–70°W, averaged over 5°S–5°N). The displayed value is the deviation of monthly climatology from its mean climate. The impact of the improved mean climate on the seasonal cycle of SST is shown in Fig. 4a. Since a time-independent surface heat flux adjustment is applied to the model, it is not surprising that it could improve the mean climate of SSTs as shown in Sect. 4.1. Yet, it is not necessary that the seasonal cycle of SSTs will also be improved by this procedure. However, we notice that the seasonal cycle of equatorial SST in FLX is significantly improved relative to CTL. As shown in Fig. 4a, CTL produces an unrealistic semi-annual cycle in the eastern Pacific without any indication of observed westward propagation. In contrast, FLX simulates the observations reasonably well with a pronounced annual cycle and a westward propagation in the eastern Pacific. These improvements in mean climate and seasonal cycle agree with Xie (1994) and Li and Philander (1996) who found that the north–south asymmetric structure is crucial to determine a dominant annual cycle in the eastern Pacific.

The improved SST seasonal cycle is closely linked to improvements in other variables. Figure 4b shows the seasonal cycle of the wind speed, represented by the magnitude of the surface wind stress. It is interesting that the pattern of the seasonal cycle of wind speed resembles that of SST (see Fig. 4a) both in observations and the two

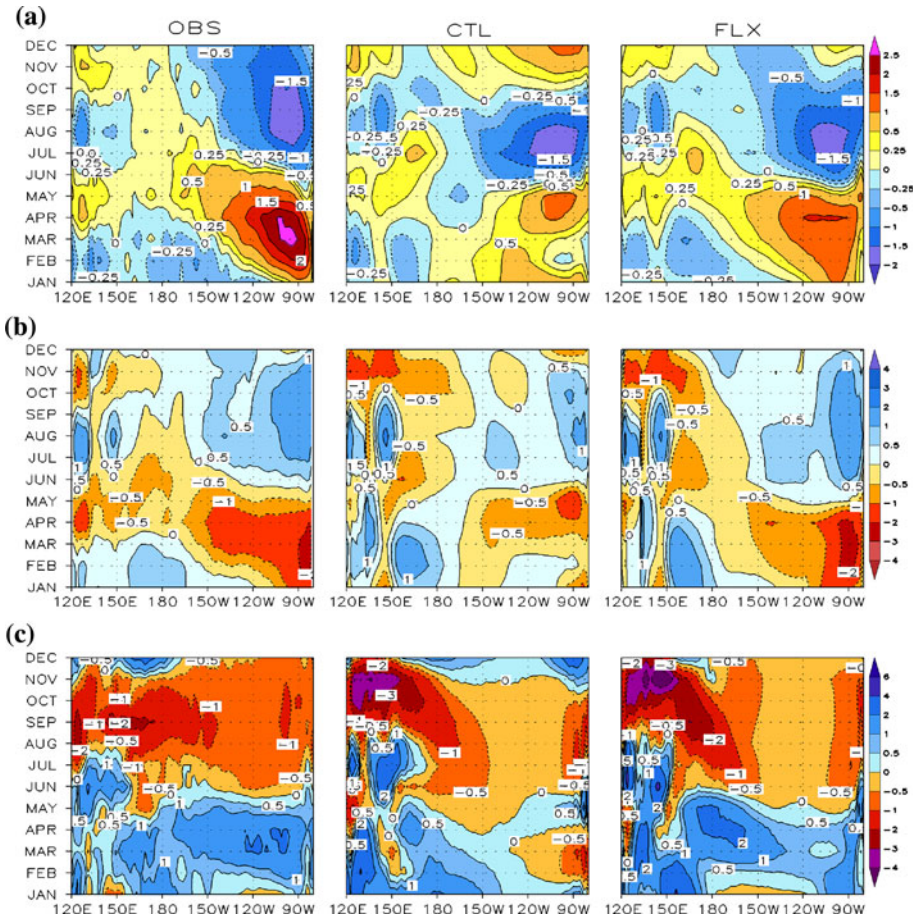

Fig. 4 Seasonal cycle of **a** SSTs (°C), **b** wind speed (m s^{-1}) and **c** precipitation (mm day^{-1}) along the equatorial Pacific region (averaged over 5°S–5°N) for OBS, CTL and FLX. The mean climate is removed. In *each panel*, the *vertical axis* indicates the month-of-year, varying from the *bottom* to *top*

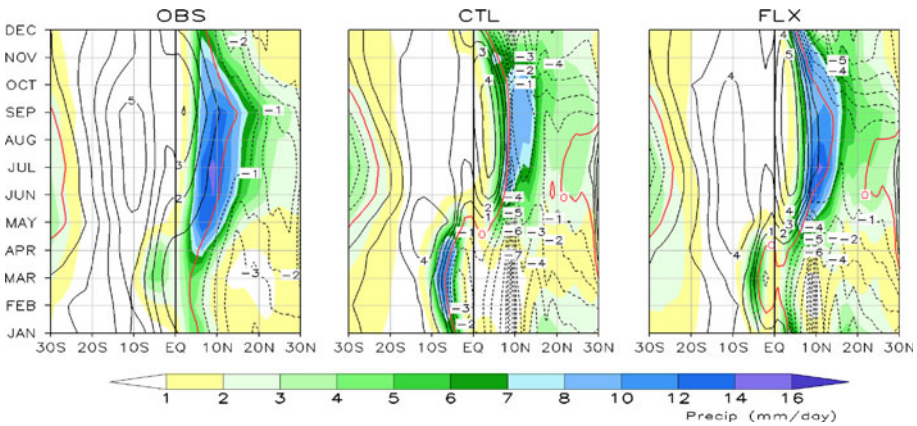

Fig. 5 Seasonal cycle of total precipitation (mm day^{-1}) and total meridonal wind stress (0.01 N m^{-2}) in the eastern Pacific area (zonally averaged over 120°W–80°W) for OBS, CTL and FLX. In *each panel*, the *vertical axis* indicates the month of year, varying from the *bottom* to *top*. *Shadings* represent total precipitation and contours represent total meridional wind stress with zero lines in *red*

simulations. In the observations and FLX both wind speed and SST exhibit robust annual cycles that are dominant in the eastern Pacific with westward propagation over the eastern and central Pacific in the first half of year. In CTL, both wind speed and SST exhibit an erroneous semiannual cycle in the eastern Pacific. The similarity in wind speed and SST implies that these two quantities are strongly connected as further discussed in Fig. 6.

FLX also successfully simulates the observed annual cycle of precipitation in the eastern equatorial Pacific in comparison with an unrealistic semi-annual cycle of precipitation in CTL (Fig. 4c). This improvement of precipitation in FLX is associated with the improved meridional winds and the more realistic location of the ITCZ around the equator. As shown in Fig. 5, there is a major unrealistic feature in the seasonal cycle of the equatorial total meridional wind stress in CTL. The southerly winds (solid contours) are persistent during the entire year to the south of the equator and even slightly cross the equator in the observations. In contrast, CTL simulates strong northerly

winds (dash contours) persisting from January to March and relatively weak southerly winds (solid contours) from June to October. FLX simulates strong southerly winds from June to October as observed. Although northerly winds still exist from January to March in FLX, the intensity, with a maximum 0.01 N m^{-2}, is much weaker than 0.03 N m^{-2} in CTL, and thus the ITCZ persists mostly to the north of the equator throughout the year in FLX as observed (blue shading areas in Fig. 5).

As described above, the seasonal cycle in FLX is improved for SST, wind speed and precipitation, even though the heat flux adjustment is constant in time and no momentum and fresh water flux adjustments are applied. Therefore, these changes must be caused by improved model physical processes on seasonal time scales in response to the imposed mean heat flux adjustment. We speculate that wind-evaporation-sea surface temperature feedback is possibly responsible for these improvements. This feedback reinforces both the seasonal wind and SST anomalies through a positive feedback as in the case of the mean state. Figure 6 shows the seasonal differences of wind speed, latent heat flux (representing evaporation), SST and oceanic heat content (representing thermocline depth) between FLX and CTL (i.e. FLX minus CTL). The improvement in FLX relative to CTL is most obvious in the seasons of spring and late autumn. As indicated by Fig. 4a and b, FLX significantly reduces the erroneous cold SST and strong wind speed in CTL in spring, and reduces erroneous warm SST and weak wind speed in late autumn. In spring, the lower wind speed in the eastern Pacific in FLX (blue shadings, Fig. 6a) mainly contributes to the reduced evaporative heat loss (blue shadings, Fig. 6b) there. Correspondingly, SST is much warmer (red shadings, Fig. 6c) in this run. Consistent with the higher wind speed in FLX from May to August, the difference in evaporation peaks in June to August. However, SST becomes colder in FLX a few months later, i.e., in late autumn. The process becomes more complicated in late autumn because the subsurface oceanic dynamical processes also strongly affect SST in this season. In fact, cold heat content signals (blue shadings, Fig. 6d) occur in the western Pacific in June and propagate eastward reaching a maximum in late autumn in the eastern Pacific. This late autumn maximum is largely contemporaneous with the major surface cooling there and may be mainly responsible for the colder SST in this season in FLX.

5 ENSO-related interannual variability

This section investigates the impact of improved characteristics in the mean climate fields on the simulation of ENSO-related interannual variability. The data from the last 50 years of OBS, CTL and FLX are used for comparisons.

5.1 Temporal characteristics

Figure 7 displays the time series of the Nino3.4 SST anomaly and its standard deviation for the observations and both experiments. Highly regular (biennial) variation of ENSO in CTL is clearly seen. The standard deviation of the Nino3.4 SST anomaly for the observations, CTL and FLX are 0.83, 0.87 and 0.72°C, respectively. The difference between CTL and FLX is highly significant at a 0.01 significant level. The amplitude of ENSO events is slightly overestimated in CTL, while underestimated in FLX. The weakened ENSO amplitude in FLX might be associated with the damping effect caused by constantly applying the heat flux adjustment. The damped ENSO is also found by Spencer et al. (2007), where a heat flux adjustment was

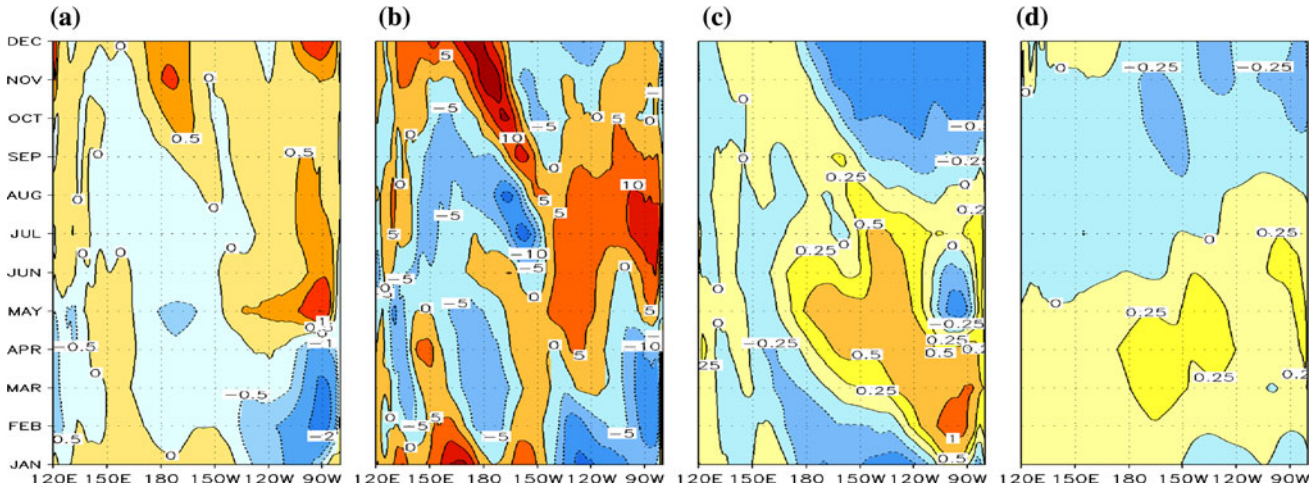

Fig. 6 Difference between FLX and CTL (FLX–CTL) for seasonal cycle of **a** wind speed (m s^{-1}), **b** latent heat flux (W m^{-2}), **c** SST (°C) and **d** heat content (°C) along the equatorial Pacific region (averaged over 5°S–5°N). The mean climate is removed

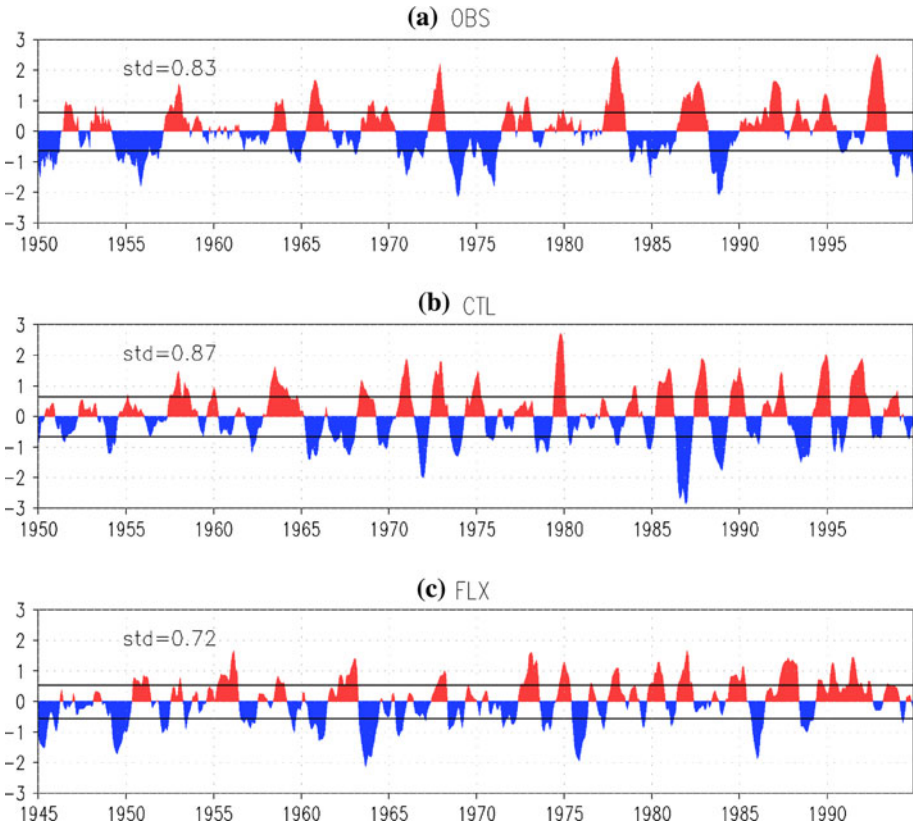

Fig. 7 50-year time series of monthly SSTs anomalies with seasonal cycle removed (°C) in the Nino3.4 region for **a** OBS, **b** CTL, **c** FLX. The standard deviation is shown in *left corner*. The *thin straight lines* in *each panel* refer to plus and minus 3/4 standard deviations

applied in the tropical part of HadCM3. As revealed in Spencer et al. (2007), the amplitude of ENSO variability in the model resembled that of the observed ENSO when the flux adjustment was applied only within 10° of tropics, which may be more targeted at the wind errors within the equatorial waveguide. Therefore, one suggestion to avoid the damped effect is to target the momentum and heat flux adjustment only to certain regions, such as within 10° of tropics rather than 30°. We may also limit the heat flux adjustments to the eastern ocean where the SST bias is more likely due to the incorrect surface heat balance. However, the improvement of the representation of physical processes in the models may be the real solution to eliminate the model bias. Figure 8a presents the power spectrum of the 50-year Nino3.4 SST anomaly index for the observations and both CTL and FLX. A broad band with a period ranging from 1.2 to 4.5 years is seen in the observations. The dominant period in the observations is about 4 years, with a secondary quasi-biennial peak. CTL exhibits a distinct and robust quasi-biennial oscillation (see also Fig. 7b), which is a major deficiency of CCSM3 (Deser et al. 2006). In contrast, the biennial variability is absent in FLX and replaced by a dominant period of 2.6 years and a secondary dominant period of 1.7 years under a broader spectral band more like the observations. However, the overall area under the spectral density curve in FLX is much less than that in the observations and CTL,

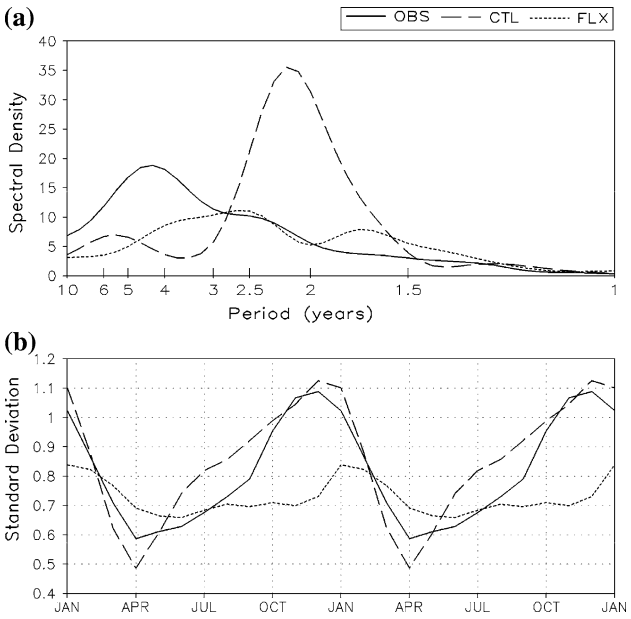

Fig. 8 **a** Power spectrum of 50-year Nino3.4 SST anomaly index and **b** two repetitions of the standard deviation of the Nino3.4 SST anomaly index (°C) as the function of the calendar month for OBS (*solid line*); CTL (*long dash line*); FLX (*short dash line*)

indicating that the amplitude of ENSO variability is reduced in FLX. It is consistent with the result from the standard deviation in Fig. 7.

The standard deviation of the Nino3.4 SST anomaly as a function of the calendar month (Fig. 8b) indicates that the observed interannual variability has the weakest amplitude of 0.59°C in the boreal spring (around April) when the ENSO events usually just start or vanish, and has the strongest amplitude of 1.1°C in the boreal winter (around December) when the ENSO events usually peak. CTL simulates well the observed phase locking to the seasonal cycle, while FLX gives a weak and delayed preference of phase locking to the seasonal cycle, i.e., a hint of the minimum 0.65°C during June and the maximum 0.84°C during January, 1 or 2 months later than the observations and CTL. This discrepancy is likely associated with the fact that SST anomalies are damped too quickly in FLX.

5.2 Spatial structure

The spatial distributions of the standard deviation of the monthly SST anomaly for the observations and the two experiments are compared in Fig. 9a. It shows that the observed SST variation is large in the tropical cold tongue region which is enclosed by the 24°C isotherm in the annual mean field (Fig. 1a). Maximum variability occurs in the eastern equatorial Pacific and off the coast of Peru. CTL gives a realistic amplitude of the largest SST variation of 1.25°C, while FLX clearly underestimates the SST variability by 0.25°C. It is found that both experiments have the common deficiency of not simulating the location of the maximum SST variability in the eastern Pacific Ocean off the Peru coast although the mean climate biases are largely reduced in FLX. This is likely associated with the fundamental mean climate biases of the thermocline depth in the cold tongue region along the equator and off the coast of Peru in CCSM3 (e.g. Deser et al. 2006). The maximum off the coast of Peru is not reproduced corresponding to the presence of the warm bias there (Fig. 1d, f) in both CTL and FLX. Maximum SST variability in both simulations resides away from the coast of Peru, and is displaced westward of the observed maximum. This bias is consistent with the westward displacement of the cold tongue in the mean climate (Fig. 1c, e). The area of the largest variability is confined too closely to the equator. Although FLX is able to simulate a more realistic mean

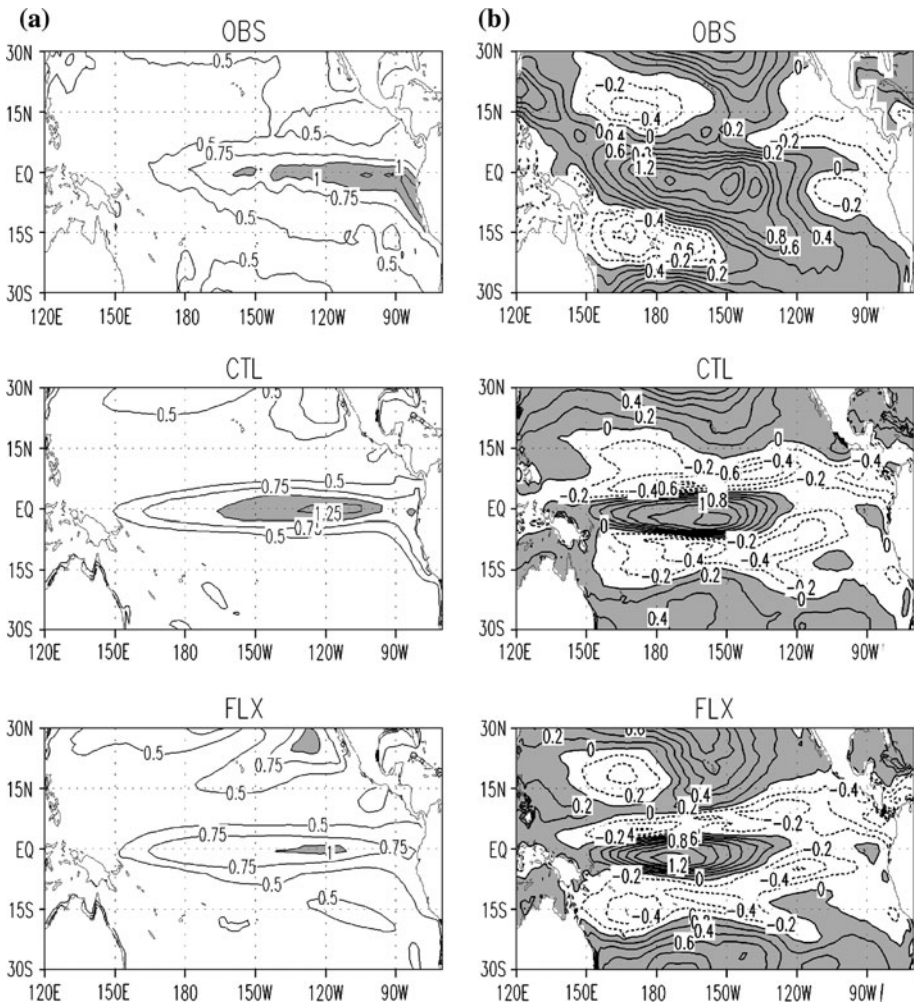

Fig. 9 Spatial distributions of **a** SST standard deviation (°C) and **b** coefficients of the linear regression of monthly zonal wind stress anomaly onto the corresponding Nino3.4 SST anomaly (0.01 N m^{-2} K^{-1}) over the tropical Pacific for OBS, CTL and FLX. The shaded areas represent the values larger than 1 in **a** and larger than zero in **b**. The interval is 0.25°C in **a** and 0.002 N m^{-2} K^{-1} in **b**

climate in the eastern equatorial Pacific and off the coast of Peru (refer to Fig. 1f, Fig. 2f and Fig. 3), the heat flux adjustment is not effective in improving the spatial distribution of the interannual variability which is partly driven by subsurface temperature anomalies associated with the thermocline fluctuation.

In order to further investigate the reason for the meridional confinement of the ENSO variability in the model, the zonal wind stress anomaly is regressed onto the Nino3.4 SST index. As shown in Fig. 9b, both simulations capture the observed westerly anomaly (shaded area) in the central Pacific during a warm event. The amplitude of the maxima 0.014 N m^{-2} K^{-1} is also comparable to the observed value in the central equatorial Pacific. However, compared to about 15°S–15°N in the observation, the westerly anomaly in both simulations is meridionally confined to the equator 7°S–7°N although FLX shows slightly broader distribution. It indicates that the narrow meridional span of zonal wind stress anomaly is also responsible for the problem of the meridional confinement with CCSM3. Deser et al. (2006) found that the high frequency of the interannual variability in CCSM3 is associated with this problem of the meridional confinement.

5.3 Evolution

Based on the Bjerknes (1969) positive feedback mechanism, a warm (cold) ENSO event will occur if the easterly wind is weakened (strengthened). This causes the deepening (shoaling) of the thermocline depth in the eastern Pacific, and further warming (cooling) of the sea surface. Figure 10 shows the

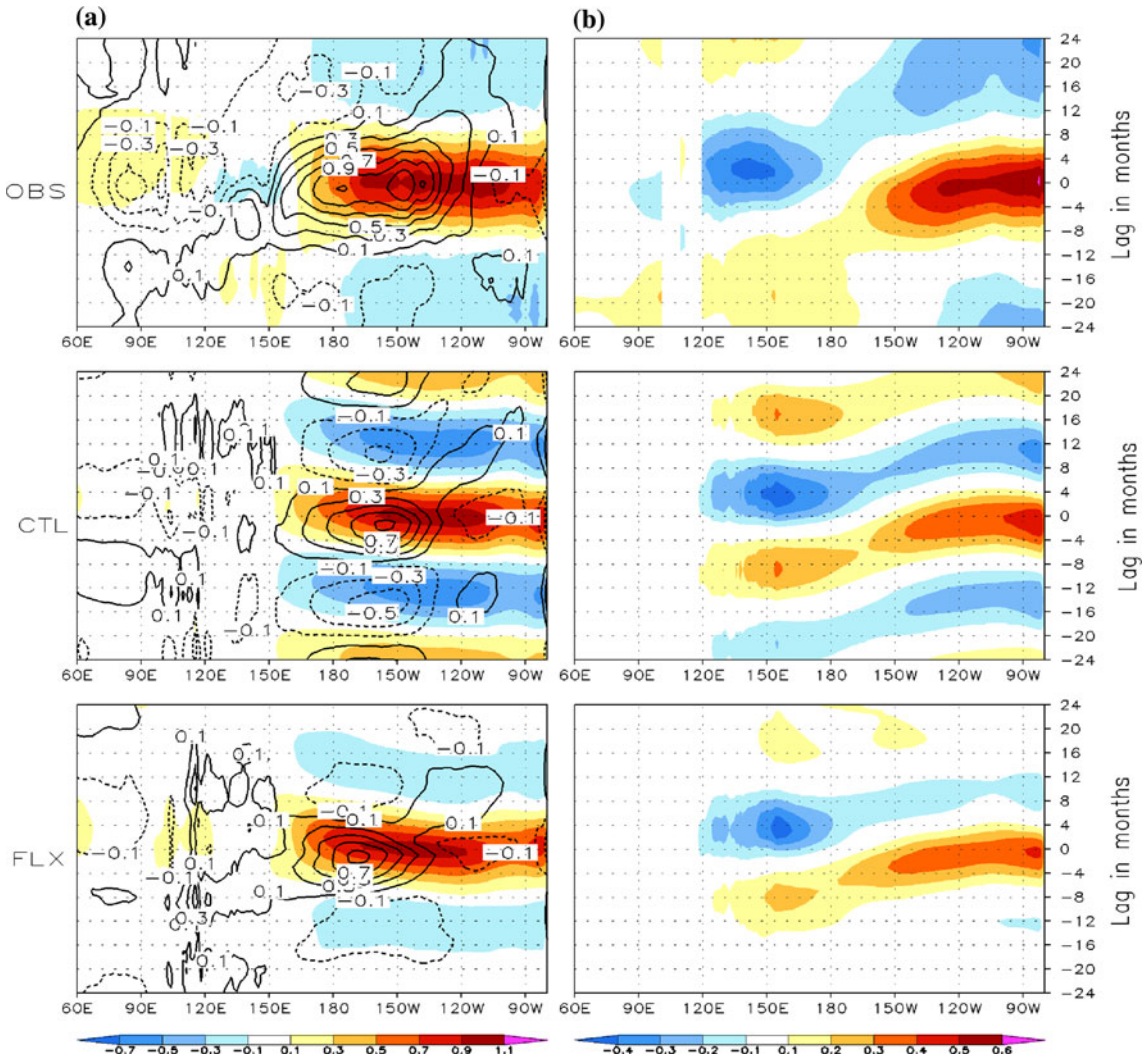

Fig. 10 Coefficients of the linear lead/lag regression of variables onto the Nino3.4 SST anomaly. *Columns* correspond to the regressions for the monthly **a** SST anomaly (K K^{-1}) in shadings and zonal wind stress anomaly (0.01 N m^{-2} K^{-1}) in contour, and **b** Heat content anomaly (K K^{-1}) in shadings along the equator (averaged over 5°S–5°N). The positive in *y*-axis corresponds to the variable lagging Nino3.4 SST anomaly in months, and the negative corresponds to the variable leading Nino3.4 SST anomaly in months. Lag-0 indicates the peak of ENSO events. Intervals are 0.002 N m^{-2} K^{-1} for zonal wind stress anomaly in **a**

temporal evolution of SST, zonal wind stress, and heat content during the ENSO events. Linear 24-month lead/lag regressions of 50-year monthly tropical SST, zonal wind stress and heat content anomalies along the equatorial Pacific and Indian Ocean (average of 5°S–5°N) onto the Nino3.4 SST anomaly index over a 48-month period are provided.

Some improvements of FLX over CTL are demonstrated. It includes a more realistic ENSO evolution in FLX. FLX does not show strong biennial oscillations in SST, zonal wind stress (Fig. 10a) and heat content (Fig. 10b), whereas CTL does. However, we found a main problem with CCSM3, i.e. a weak Bjerkness positive feedback in the central and eastern equatorial Pacific (east of 150°W). This problem includes the early peaking of the wind stress anomalies and the confinement of its center in the ENSO growth and maturation phases. This suggests a weak coupling strength between wind stress and SST. The observed coherent eastward expansion of wind stress anomalies shown in the ENSO mature phase is weakened in both simulations. The magnitude of the maximum of wind stress anomaly is weaker in CTL and FLX than that in observations, and the maximum of heat content in the eastern Pacific is also underestimated in both simulations. The underestimated heat content indicates a weak response in the subsurface ocean of CCSM3.

We also looked at the evolution of the composite cold and warm events separately for both CTL and FLX (not shown). We found that the duration and intensity of the cold events were comparable with those of the warm events in FLX, which is similar to CTL. Therefore, the asymmetric damping effect between cold and warm events seems to be small in FLX. This is probably because the new mean state in FLX, on which the anomalies are defined, has absorbed most of the effect of the heat flux adjustment.

6 ENSO prediction

In this section we describe results from two sets of hindcasts. The first set of hindcasts is conducted using the CTL version of the CCSM3, the second set using the FLX version of the CCSM3. In this study only SST is analyzed. We refer to hindcasts by their initial month, e.g., "January hindcasts" denote those hindcasts initialized on 1st January. The 1-month lead-time refers to the first monthly mean, e.g., the average of January in January hindcasts. Similarly, the 2-month lead-time refers to the second monthly mean, e.g., the average of February in January hindcasts.

In terms of the mean climate of the ensemble mean monthly SST during the period 1982–1998, the difference of CTL hindcasts from the observation and the difference of FLX from CTL hindcasts in both January and July hindcasts are shown in Fig. 11a and b, respectively. OBS can be referred to Fig. 1a. The January and July FLX hindcasts exhibit a reduced warming bias (<1°C) off the coast of South America relative to their CTL counterparts. The January and July FLX hindcasts also exhibit less systematic error in the seasonal cycle of SST in the equatorial Pacific than do the corresponding CTL hindcast (Fig. 12). The January FLX hindcasts show reduced warming bias (up to 0.5–1°C) throughout the year in the eastern Pacific, and slightly reduced cold systematic error

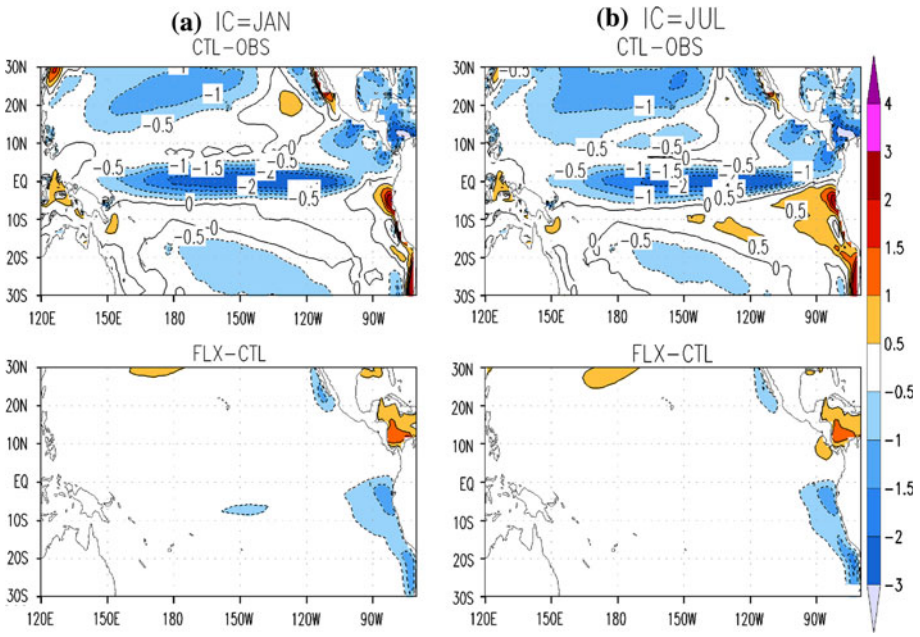

Fig. 11 The differences of mean climate of ensemble mean monthly SST (°C) between CTL hindcasts and OBS (*upper panels*), and between FLX and CTL hindcasts (*lower panels*) over the Pacific for the period of 1982–1998. **a** is for January hindcast, and **b** is for July hindcast

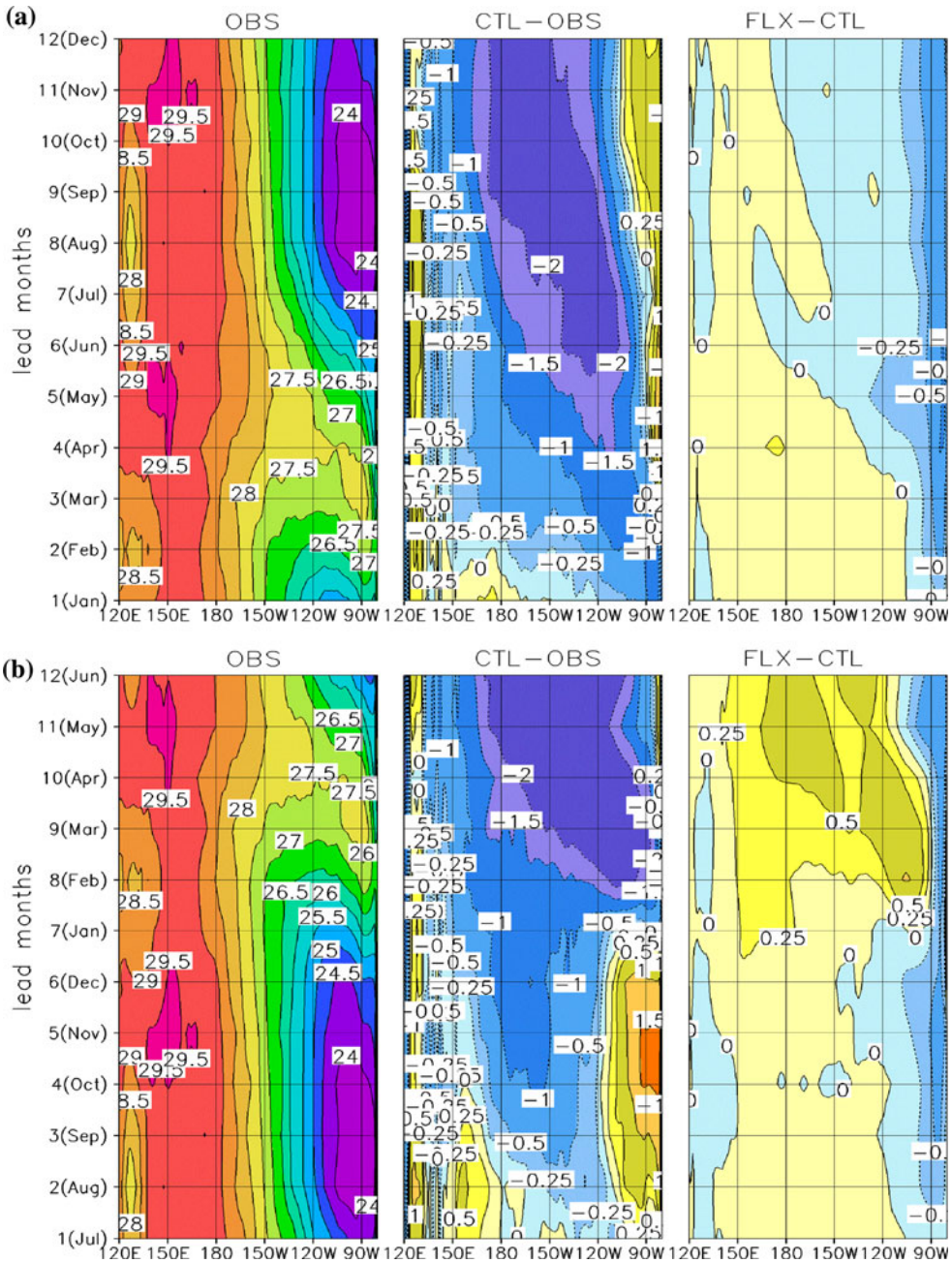

Fig. 12 Seasonal variation of ensemble mean monthly SST (°C) at the equatorial Pacific (averaged over of 5°S–5°N) for OBS, difference of CTL from OBS, difference of FLX from CTL over the period of 1982–1998. **a** Is for January hindcast, and **b** is for July hindcast

(<0.5°C) at the first 5-month lead-time but increased cold error (<0.5°C) at 6–12 month lead-time in the central Pacific. The July FLX hindcasts display a reduced warming bias in the eastern Pacific (<0.5°C) and reduced cold systematic error (<1°C) almost throughout the year in the central Pacific.

The skill of the hindcasts is measured by the anomaly correlation coefficient (ACC) and the root mean square error (RMSE) of the Nino 3.4 SST index against the corresponding observations as shown in Fig. 13. The ACC measures the similarities in evolution of the hindcasts and the observations and the RMSE measures the magnitude of the difference between the observed and hindcasted time series. Note that both hindcasts and the observations are represented by the deviations from their corresponding monthly climatology. For convenience, we refer to ACC >0.6 as a skillful level (see Kirtman and Zebiak 1997), while noting that such choice is highly subjective.

Figure 13a gives the skill score for the January hindcast as a function of the lead-time. The skill score of a persistence hindcast is also shown (in black) as a reference of a baseline skill. In general, skill scores of both CTL (in blue) and FLX (in red) hindcasts drop steadily as the lead time increases, especially during the first 4 months. Both FLX

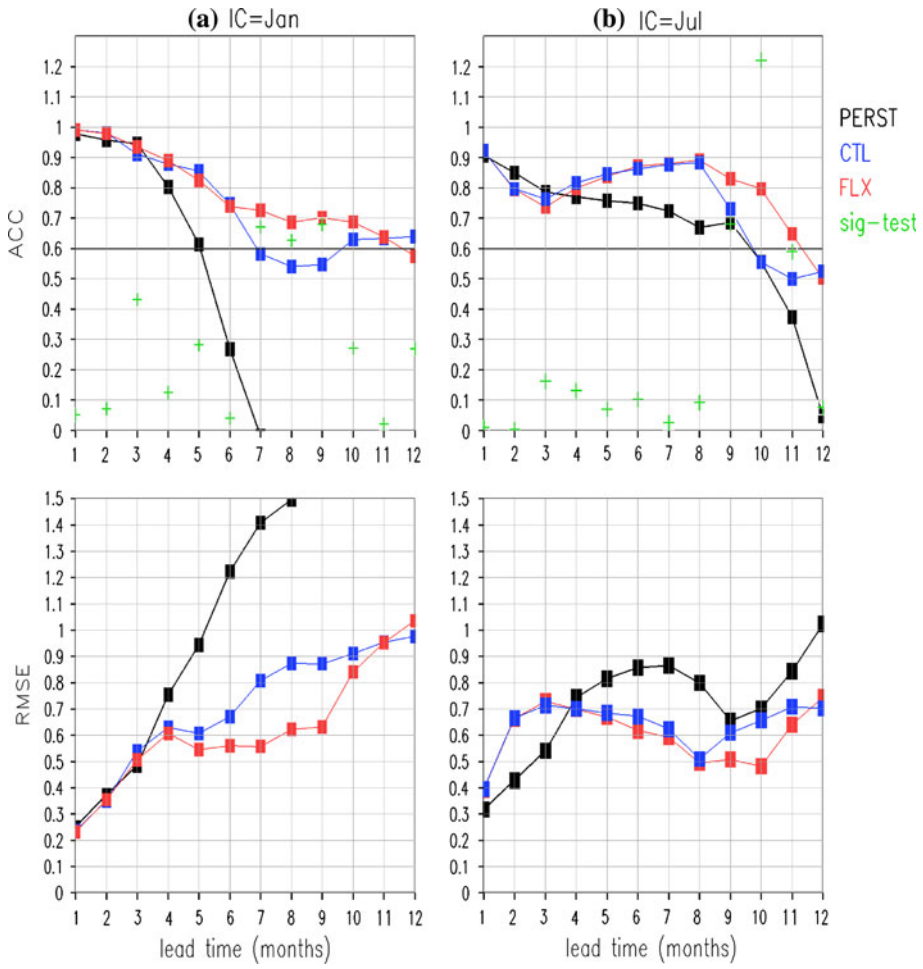

Fig. 13 Prediction skill measured by anomaly correlation coefficient (ACC) and root mean square error (RMSE) for **a** January and **b** July initialized hindcast from 1982 to 1998 using the Nino3.4 SSTA index. The skill of the persistence hindcast is denoted by *black curve*, and the ensemble mean FLX is denoted by *red curve* and CTL by *blue curve*. ACC above 0.6, *line* indicates a skillful hindcast. In the *panel* of ACC, the *green cross* represents the standardized difference of the hindcast skill between FLX and CTL at each lead-time

and CTL are more skillful than the persistence hindcast beyond the first 3 months. FLX hindcasts are skillful for the first 10 months (score above 0.6) and CTL hindcasts are skillful only for the first 6 months. At a 6-month lead-time, the skill scores for both CTL and FLX hindcasts are relatively high (>0.7), but are indistinguishable from each other. At longer lead times of 7–9 months, FLX hindcasts have higher skill (about 0.2 greater) than CTL hindcasts. The RMSE show consistent results. CTL and FLX hindcasts have comparable error in the first 6 months, while CTL hindcasts have larger errors of up to 0.3°C at the lead-time of 7–9 months. The significance of the difference between CTL and FLX in ACC is tested, based on a one-tailed Gaussian distribution, by first applying a Fisher's Z transformation to convert these two samples of correlations to a Gaussian distribution (refer to http://davidmlane.com/hyperstat/B8712.html). The score of the sample statistic is denoted by the green cross in ACC plot. The difference between CTL and FLX at the lead-time of 7–9 months is statistically significant at a 45% confidence level when the green cross is >0.6. Since the 45% confidence level is quite low, we claim that this difference between the two sets of hindcasts is not statistically significant. These results are limited by the small numbers of cases and ensemble size, which span only 17 years and three members, respectively. In future work, a larger number of cases and ensemble members should be included to test the robustness of these results.

The skill of the July hindcasts is shown in Fig. 13b. FLX hindcasts exceed 0.6 for lead-time of 0–11 months, whereas CTL hindcasts are skillful only for the first 9 months. Both have similar skill in the first 8-month lead-time. After that time, the hindcast skill drops rapidly in CTL hindcast. At 9–11 months lead time, FLX hindcasts have higher skill than CTL hindcasts with a higher ACC and lower RMSE up to 0.2 and 0.2°C, respectively. The difference between FLX and CTL is statistically significant at a 45% confidence level at 9 and 11 months lead-time and 77% at 10-month lead time as denoted by the green crosses >0.6 and 1.2 in ACC plot.

This increased July FLX hindcast skill at 9–11 month lead-time is likely associated with the improved seasonal cycle during the same period (Fig. 12b). This improvement can be attributed to the reduced SST bias in boreal spring

by the heat flux adjustment. Nevertheless, it is not the case for the January FLX hindcast. Although the bias correction is largest in about the same calendar months, its impact is much smaller.

7 Summary and discussions

The impact of mean climate on the seasonal cycle and ENSO simulation and hindcast skill has been investigated by applying a time-independent surface heat flux adjustment in CCSM3. The resulting mean climate, seasonal cycle, ENSO simulation and ENSO hindcast skill determined in cases where the heat flux is adjusted (FLX) are compared with those without the heat flux adjustment (CTL).

Some new and unique aspects of this study are as follows: (1) the results of this study are based on a state-of-the-art coupled model (CCSM3); (2) all experiments analyzed in this study are forced by the anthropogenic and natural forcing over the twentieth century; and (3) the impact of heat flux adjustment is investigated not only on ENSO simulation but also on ENSO hindcast.

The results show that mean climate is overall improved in the heat flux-adjusted simulation. In particular, the warm biases off the coast of Peru are reduced. The simulation of the cross-equatorial southerly winds in the eastern Pacific is also improved and as a result the double ITCZ is less pronounced. The cold biases in the central equatorial Pacific are also reduced and extend less westward. Thus, the east–west and particularly north–south asymmetric structures of mean climate in tropical Pacific are better represented in the flux-adjusted model. A positive wind-evaporation-sea surface temperature feedback, triggered by the heat flux adjustment, physically contributes to this outcome.

As a major benefit of this improved mean climate in the flux-adjusted simulation, a more realistic annual cycle of SST with westward propagation is simulated. A more realistic wind speed annual cycle is also simulated despite no momentum flux adjustment applied. It helps to make precipitation patterns varying with season more realistically. Since the heat flux adjustment is constant in time and no momentum and fresh water flux are applied, these changes in wind speed and precipitation are caused by improved model physical processes on seasonal time scales in response to the heat flux adjustment and improved mean climate. It is found that the more realistic latent heat flux associated with the surface wind is responsible for the improvement in the spring season and the more realistic oceanic heat content can explain the improvement in the late fall season. This study implies that, if the mean climate is represented well in a model such as CCSM3, the model can generate a realistic annual cycle in the eastern equatorial Pacific Ocean, with the current excessive semi-annual components largely eliminated.

Our results demonstrate that the model ENSO is sensitive to these modifications in the mean climate and seasonal cycle. In the control experiment, the Nino3.4 SST index is regular and biennial. By contrast, it is less regular in the flux-adjusted experiment. Some theoretical work (Jin et al. 1994; Tziperman et al. 1994) implied that ENSO is phase-locked to the seasonal cycle (i.e. locking of peaking anomalies to the boreal winter) and the system irregularly jumps among different nonlinear resonances with the seasonal cycle that might determine the spectrum and aperiodic nature of ENSO. Therefore, it is likely that the modification in the ENSO period in the flux-adjusted simulation is related to the interaction between the more realistic annual cycle and interannual variability in the eastern equatorial Pacific.

Our results show that mean climate can cause changes in ENSO variability, and ENSO variability clearly has some non-linear dependencies. However, the interaction of mean climate with ENSO is model-dependent. The overall results in this study show that a more realistic mean climate in CCSM3 produces a more realistic seasonal cycle. The simulation of ENSO variability is improved in some ways (e.g. it becomes more irregular), but gets worse in some other aspects (e.g. the phase-locking to the seasonal cycle is weak and the amplitude of ENSO variability is reduced). Compared with the result of Manganello and Huang (2009), who used a similar heat flux scheme in the Center for Ocean–Land–Atmosphere Studies (COLA) CGCM, some features of ENSO were improved in their model (e.g. the phase-locking to the seasonal cycle is close to the observed), but not so in CCSM3, even though the mean climate and seasonal cycle in both heat flux-adjusted models are improved. Moreover, the previous studies have shown that the relationship between the mean climate and interannual variability varies with models, based on results using multimodels (Neelin et al. 1992; Mechoso et al. 1995; Latif et al. 2001; AchutaRao and Sperber 2002). Some models with a realistic mean climate reproduced many observed ENSO features, while others with a realistic mean climate failed to do so. This is due in part to the fact that the interannual variability is a non-linear process and more than one active mechanism determines the behavior of ENSO variability (Delecluse et al. 1998). Moreover, the coupling process between individual climate components is still not fully understood (Fedorov and Philander 2000).

This study indicates that the impact of mean climate on ENSO hindcast skill is small and not statistical significant. The flux-adjusted hindcasts show slightly higher hindcast skill than the control hindcasts at 7–9 month lead-time in the hindcasts initialized in January and 9–11 month lead-

time in the hindcasts initialized in July. Their differences at these lead times are significant at a 45% confidence level. This is partly due to the limitation of the size of cases and ensembles. Although the statistical significance is low, our preliminary hindcasts may provide useful hints about how to use CCSM as a climate forecast system. Delsole et al. (2008) also implemented three empirical methods to reduce the systematic error in their coupled land–atmosphere model. They concluded that none of these methods improved the forecast skill of the model even though the systematic error is reduced. Therefore, a suggestion based on the result from our study in addition to the conclusion drawn by Delsole et al. (2008) is that removing systematic error of coupled models by heat flux adjustment or other empirical methods may not improve the ENSO hindcast skill. Clearly, what is needed is a fundamental focus on the improvement of the representation of physical processes that would improve the fidelity of the models.

Acknowledgments This paper is based on the first author's Ph.D. dissertation. The first author greatly appreciates her other advisory committee members, B. Kirtman and E. Schneider, for their guidance and support throughout her dissertation research. In addition, the authors have benefited from discussions with K. Pegion and J. Manganello. We would also like to thank B. Kirtman and D. Min for providing ocean initial conditions for the hindcast experiments. We would like to thank the three anonymous reviewers, who made very helpful suggestions to revise the paper. Their comments have improved the paper. We acknowledge the National Center for Atmospheric Research (NCAR) for providing the Climate Community System Model (CCSM) and its control simulation output. In particular, Buja Lawrence and Gokhan Danabasoglu gave valuable guidance for the model setup. We are also grateful to the NCAR Computational and Informational Systems Laboratory for providing computing resources and technical support. This research was supported by the National Science Foundation (ATM0332910, ATM0830062, ATM0830068), National Aeronautics and Space Administration (NNG04GG46G, NNX09AN50G), and the National Oceanic and Atmospheric Administration (NA04OAR4310034, NA09OAR4310058). B. Huang was also supported by the funding from NOAA CVP Program (NA07OAR4310310).

References

AchutaRao K, Sperber K (2002) Simulation of the El Niño Southern Oscillation: results from the coupled model intercomparison project. Clim Dyn 19:191–209

Annamalai H, Hamilton K, Sperber KR (2007) The South Asian Summer Monsoon and its relationship with ENSO in the IPCC AR4 simulations. J Clim 20:1071–1109

Bjerknes J (1969) Atmospheric teleconnections from the equatorial Pacific. Mon Weather Rev 97:163–172

Collins WD et al (2006) The Community Climate System Model Version 3 (CCSM3). J Clim 19:2122–2143

Davey M, Huddleston M, Sperber KR et al (2002) STOIC: a study of coupled model climatology and variability in tropical ocean regions. Clim Dyn 18:403–420

Delecluse P et al (1998) Coupled general circulation modeling of the tropical Pacific. J Geophys Res 103(C7):14357–14373

DelSole T, Zhao M, Dirmeyer PA, Kirtman BP (2008) Empirical correction of a coupled land–atmosphere model. Mon Weather Rev 136:4063–4076

Derber J, Rosati A (1989) A global oceanic data assimilation system. J Phys Oceanogr 19:1333–1347

Deser C, Capotondi A, Saravanan R, Phillips A (2006) Tropical Pacific and Atlantic climate variability in CCSM3. J Clim 19:2451–2481

Doney SC, Large WG, Bryan FO (1998) Surface ocean fluxes and water-mass transformation rates in the coupled NCAR Climate System Model. J Clim 11:1420–1441

Fedorov AV, Philander SG (2000) Is El Niño changing? Science 288:1997–2002

Jin FF, Neelin JD, Ghil M (1994) El Niño on the Devil's staircase: annual subharmonic steps to chaos. Science 264:70–72

Joseph R, Nigam S (2006) ENSO evolution and teleconnections in IPCC's twentieth-century climate simulations: realistic representation? J Clim 19:4360–4377

Kalnay E et al (1996) The NCEP/NCAR 40-year reanalysis project. Bull Am Meteorol Soc 77:437–471

Kirtman BP, Min D (2009) Multi-model ensemble ENSO prediction with CCSM and CFS. Mon Weather Rev 137:2908–2930

Kirtman BP, Zebiak SE (1997) ENSO simulation and prediction with a hybrid coupled model. Mon Weather Rev 125:2620–2641

Latif M et al (1994) A review of ENSO prediction studies. Clim Dyn 9:167–179

Latif M et al (2001) ENSIP: intercomparison project. Clim Dyn 18:255–276

Leloup J, Lengaigne M, Boulanger J (2008) Twentieth century ENSO characteristics in the IPCC database. Clim Dyn 30(2–3):277

Li T, Hogan TF (1999) The role of the annual-mean climate on seasonal and interannual variability of the tropical pacific in a coupled GCM. J Clim 12:780–792

Li T, Philander SGH (1996) On the annual cycle of the eastern equatorial Pacific. J Clim 9:2986–2998

Lin JL (2007) The double-ITCZ problem in IPCC AR4 coupled GCMs: ocean–atmosphere feedback analysis. J Clim 20:4497–4525

Manganello J, Huang B (2009) The influence of systematic errors in the Southeast Pacific on ENSO variability and prediction in a coupled GCM. Clim Dyn 32(7–8):1015–1034

Mechoso CR et al (1995) The seasonal cycle over the tropical Pacific in general circulation models. Mon Weather Rev 123:2825–2838

Meehl GA, Covey C, McAvaney B, Latif M, Stouffer RJ (2005) Overview of the coupled model intercomparison project. Bull Am Meteorol Soc 86:89–93

Neelin JD et al (1992) Tropical air–sea interaction in general circulation models. Clim Dyn 7(2):73–104

Rayner NA et al (2003) Global analyses of sea surface temperature, sea ice, and night marine air temperature since the late nineteenth century. J Geophys Res 108(D14):4407–4437

Shukla J (1998) Predictability in the midst of chaos: a scientific basis for climate forecasting. Science 282:728–731

Spencer H, Sutton R, Slingo JM (2007) El Niño in a coupled climate model: sensitivity to changes in mean state induced by heat flux and wind stress corrections. J Clim 20:2273–2298

Tziperman E, Stone L, Cane MA, Jarosh H (1994) El Niño Chaos: overlapping of resonances between the seasonal cycle and the Pacific ocean–atmosphere oscillator. Science 264:72–74

Xie SP (1994) On the genesis of the equatorial annual cycle. J Clim 7:2008–2013

Xie P, Arkin PA (1997) Global precipitation: a 17-year monthly analysis based on gauge observations, satellite estimates, and numerical model outputs. Bull Am Meteorol Soc 78:2539–2558

Zebiak SE, Cane MA (1987) A model El Niño-Southern oscillation. Mon Weather Rev 115:2262–2278